JOURNAL OF Applied Polymer SCIENCE

Rubber-Toughened PLA Blends with Low Thermal Expansion

Jiandi Jiang, Lili Su, Kun Zhang, Guozhang Wu
Shanghai Key Laboratory of Advanced Polymeric Materials, School of Materials Science & Engineering, East China University of Science & Technology, Shanghai 200237, People's Republic of China
Correspondence to: Dr. G. Wu (E-mail: wgz@ecust.edu.cn)

ABSTRACT: In this study, poly (lactic acid) (PLA) blended with various rubber components, i.e., poly (ethylene-glycidyl methacrylate) (EGMA), maleic anhydride grafted poly(styrene-ethylene/butylene-styrene) triblock elastomer (*m*-SEBS), and poly(ethylene-*co*-octene) (EOR), was investigated. It was observed that EGMA is highly compatible due to its reaction with PLA. *m*-SEBS is less compatible with PLA and EOR is incompatible with PLA. Electron microscopy (SEM and TEM) revealed that a fine co-continuous microlayer structure is formed in the injection-molded PLA/EGMA blends. This leads to polymer blends with high toughness and very low linear thermal expansion both in the flow direction and in the transverse direction. The microlayer thickness of rubber in PLA blends was found to play key roles in reducing the linear thermal expansion and achieving high toughness of the blends. © 2012 Wiley Periodicals, Inc. J. Appl. Polym. Sci. 128: 3993–4000, 2013

KEYWORDS: blends; compatibilization; morphology; thermal properties

Received 22 August 2012; accepted 25 September 2012; published online 16 October 2012
DOI: 10.1002/app.38642

INTRODUCTION

Poly (lactic acid) (PLA) has attracted much attention due to the environmental concerns and sustainability issues associated with petroleum-based polymers.[1] The extrusion grade of PLA behaves high strength and modulus compared to many petroleum-based plastics. However, inherent brittleness, lack of reactive side-chain groups, and poor processing ability limit the application of PLA. The successful implementation of PLA in consumer and biomedical applications relies not only on mechanical properties being better than or comparable to conventional plastics but also on the thermal expansion behaviors. Blending is probably the most extensively used methodology to improve PLA mechanical properties. In literature, PLA has been blended with different plasticizers and polymers (biodegradable or non-biodegradable) to achieve desired mechanical properties, such as PEGs,[2] LDPE,[3] PVAC,[4] PMMA,[5] poly(ethylene-*co*-octene) (EOR),[6] poly (ethylene-glycidyl methacrylate) (EGMA),[7] PCL,[8] PBAT,[9] natural rubber,[10] isocyanate-terminated prepolymer of polybutadiene,[11] and cellulose.[12] These PLA blends universally display a significant increase in elongation compared to neat PLA. However, they yield very limited enhancement in impact strength, especially in the notched state.

Like many aliphatic polyesters, compatibilization of PLA/polyolefin blends can be achieved by several approaches, using acrylate-based copolymers,[13,14] maleic-anhydride-containing elastomers,[15–17] epoxidized polyolefins,[18,19] ethylene–vinyl acetate copolymer,[20] oxazoline-modified polymer,[21] or core–shell impact modifiers.[22,23] Recently, Oyama[7] reported super tough PLA/EGMA (80/20, w/w) blend via reactive blending. The injection-molded blends exhibited notched Charpy impact strengths which were only two to three times that of the neat PLA. After annealing at 90°C for 2.5 h, however, the impact strength of the blend increased to 72 kJ/m^2, ca. 50 times that of the neat PLA. Super-toughened PLA ternary blends with moderate strength and stiffness were also successfully prepared by melt-blending of PLA with an epoxy containing elastomer and a zinc ionomer.[24]

Due to the high thermal expansion coefficient of the rubber component, one of the major issues for the rubber-toughened PLA is how to reduce the thermal expansion coefficient so as to achieve dimensional stability. Recently, we discovered that semi-crystalline polymer/rubber blends with a co-continuous microlayer structure may exhibit a very low coefficient of linear thermal expansion (CLTE).[25,26] It was found that the viscosity ratio and compatibility of the plastic/rubber have significant effects on the CLTE, and blends consisting of the thermoplastic elastomers with high melt flow rate and excellent compatibility showed extremely low CLTE in flow direction (FD). In addition, thermal expansion of polymers appears to depend largely on the orientation degree of the crystallographic axe along the molecular chain direction. Ono et al.[27] and Kim et al.[28] confirmed the orientation of PP lamellar crystal in the injection-molded PP/rubber blend where a negative CLTE of *c*-axis orients parallel to the FD.

Table I. Materials Used

Reference	Grade name	M_n	Supplier
PLA	4032D	20,700	Natureworks LLC
EGMA	AX8900	10,000	Elf-Atochem
m-SEBS	FG1901X	-	Kraton
EOR	ENGAGE8407	-	DOW

The aim of this study is to elucidate the morphology and thermal expansion of PLA blended with epoxide or maleic anhydride functionalized rubber. Effects of rubber loading and compatibilization on the thermal expansion and impact strengths were studied, and super-toughened PLA blends with a lower thermal expansion were successfully achieved by injection molding.

EXPERIMENTAL

Materials

PLA with a stereoisomer composition of 1.2–1.6% D-isomer lactide was purchased from NatureWorks Co. A random copolymer of EGMA (Lotader AX8900) containing 24 wt % of methylacrylate and 8 wt % of glycidyl methacrylate was supplied by Elf-Atochem Co. The poly (styrene-ethylene/butylene-styrene) triblock elastomer (*m*-SEBS) used was Kraton FG1901X (supplied by Kraton Polymer), and it had been grafted with 1.84 wt % maleic-anhydride and had a molecular weight of 20,000 with a styrene content of 28 wt %. EOR rubber with the octane content of 40 wt % was supplied by DOW Chem. Co. Characteristics of these component polymers are summarized in Table I.

PLA and *m*-SEBS were dried in a vacuum oven at 80°C (EGMA and EOR at 40°C) for at least 12 h before blending. They were compounded using a twin-screw extruder (KS-20, $L/D = 44$, Kunsan, China) at a setting temperature of 180°C with a screw speed of 300 rpm. The extrudates were pelletized at the die exit. The dry pellets of the above compositions were subjected to injection molding (HTF86/TJ, China) at a cylinder temperature of 200°C, an injection pressure of 80 MPa and a mold temperature of about 50°C to prepare tensile specimens (ASTM D638, Type I) and impact bars (ASTM D256). These specimens were placed in vacuum desiccators immediately after molded for 4–6 days at 23°C before the thermal expansion testing.

Characterization

Rheological Measurements. The viscosity of polymers at various angular frequencies was measured using a rotational rheometer (RS600, Thermo Hakke, German) with a parallel plate geometry (20 mm in diameter) and a gap of 1 mm at a temperature of 180°C.

Fourier Transform Infrared Spectroscopy. Fourier transform infrared spectroscopy (FTIR) (Nicolet 5700, USA) was used to investigate the intermolecular interaction between constituents. Spectra were obtained at 4 cm^{-1} resolution and averages were obtained from 32 scans in the standard wave number range from 400 to 4000 cm^{-1}. Thin films of as-extruded PLA, EOR, *m*-SEBS and EGMA samples were prepared by casting from their dilute solutions (dichloromethane for PLA, heptane for EOR, toluene for *m*-SBES, and EGMA). For the PLA/rubber blends, the slices (400 μm in thickness) cut from as-extruded specimens were extracted in hot toluene (hot heptane for EOR) for 12 h in order to remove the free EGMA, *m*-SEBS, and EOR, respectively. A certain amount of the dried insoluble residues after the extraction was grinded with KBr powder and then compressed into discs for the FTIR test. All samples were oven-dried under vacuum to eliminate effects of residual solvent and moistures.

Morphology Observations. The morphology of cryogenically fractured specimens was observed by SEM after gold coating. A JEOL JSM-6360LV electron microscope was used at an accelerating voltage of 15 kV (Japan). The cryogenically fractured specimen was etched with heptane or toluene to remove EOR or *m*-SBES components.

To investigate the dispersion of EGMA phase in PLA, ultra-thin sections ranging from 60 to 90 nm in thickness were cryogenically cut by a diamond knife. Sections were collected on holey carbon grids and were stained with osmium tetroxide (OsO_4) vapor to enhance the phase contrast between PLA and EGMA. The thin sections were observed using a JEM-1230 transmission electron microscope (Japan).

Differential Scanning Calorimetry (DSC). The crystallinity of the PLA matrix phase can influence the thermal expansion behaviors and mechanical properties of the blends. Thermal analysis was performed using a DSC (2910 TA instrument, USA) under a nitrogen atmosphere. About 8–10 mg samples taken from the sample location in injection-molded specimens were heated to 200°C at a heating rate of 10°C/min. The crystallinity of PLA (X_c) in the injection-molded specimens was estimated by first heating cycle using the following equation:

$$X_c = \frac{\Delta H_m - \Delta H_c}{\varphi_f \Delta H_m^0} \times 100\% \quad (1)$$

where ΔH_m and ΔH_c are the enthalpies of melting and cold crystallization during the heating, respectively. Here, the value of ΔH_m^0, the heat of fusion, defined as the melting enthalpy of 100% crystalline PLA, was taken to be 93 J/g from the literature,[7] and φ_f is the weight fraction of PLA component in the blend.

X-Ray Diffraction (WAXD). WAXD was conducted using a Rigaku (D/MAX 2550, Japan) diffractometer using an incident x-ray wavelength of 1.542 A° at a scan rate of 2 deg/min in a range of $2\theta = 3$–50°. X-ray analyses were performed at room temperature.

Thermal Expansion Measurements. The CLTE was measured according to the standard of ASTM D696 using a thermomechanical analyzer (TMA2980, TA instrument, USA) under a penetration mode. To eliminate thermal history and residual stress, the injection-molded sheets were annealed at 60°C for 2 h before the test. They were then cut into rectangular specimens by milling the center part of the annealed sheets to the following dimensions: 6 mm in height [the FD], 5 mm in width [the transverse direction (TD)], and 3.2 mm in thickness [the

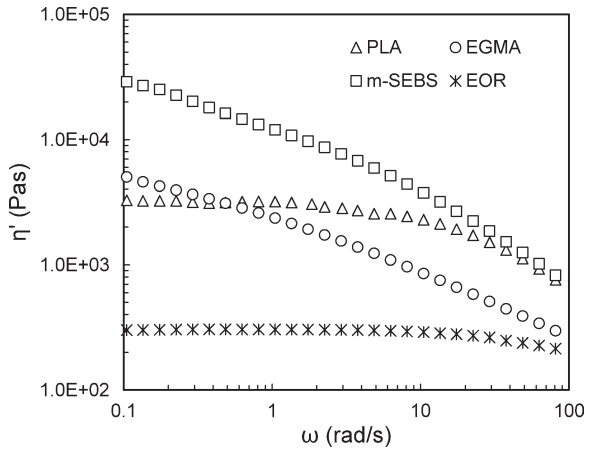

Figure 1. Dynamic viscosity of PLA and various rubbers at 180°C.

normal direction (ND)]. An average value of CLTE from −20°C to 60°C was calculated.

Impact Properties. Notched Charpy impact tests were performed at room temperature by JJ-20 memorial impact tester with a hammer of 5.5J (Changchun, China), according to ASTM D256-2000. Properties values reported here represent an average from, at least, five specimens.

RESULTS AND DISCUSSION

Rheological Properties of Raw Materials

Figure 1 shows the dynamic viscosity of PLA and three types of rubbers at 180°C. Both PLA and EOR exhibit a Newtonian plateau at low frequencies, whereas the viscosity of EGMA terpolymer and *m*-SEBS displays the shear-thinning effect in the whole frequency range. It is clear that, in the frequencies from 1 rad/s to 100 rad/s, a range of the shear rate comparable to the processing condition, the viscosity of *m*-SEBS is the highest, and then the PLA and EGMA. EOR is the lowest.

Morphology

The Morphology of Extrusion Samples. Figure 2 shows SEM and TEM images of PLA blended with 40 wt % of different rubbers. For the PLA/EOR (60/40) blend [Figure 2(a)], the dispersed domain size ranges from 20 to 30 μm. It is seen that the interface between the two phases is very smooth, indicating a completely incompatible polymer blend. We noticed that the matrix can be dissolved by hot heptane, suggesting that the dispersed domains are PLA. This is reasonable because the viscosity of EOR is much lower than that of PLA according to Figure 1. For the PLA/*m*-SEBS (60/40) blend [Figure 2(b)], due to their comparable viscosity at high frequencies, PLA appears co-continuous with *m*-SEBS. The size of the elongated domain ranges from 5 to 6 μm, indicating a poor compatibility between PLA and *m*-SEBS.

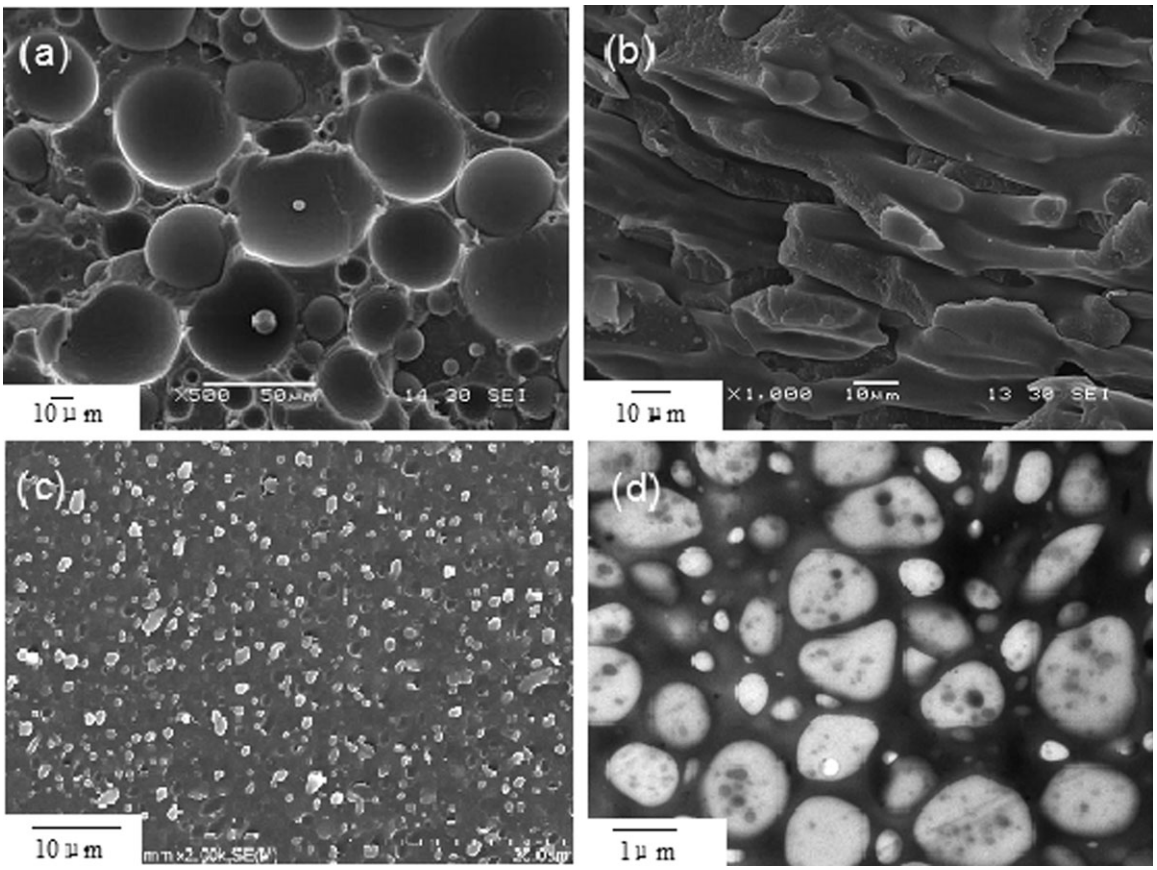

Figure 2. SEM images of the extruded PLA/rubber (60/40) blends: (a) PLA/EOR, (b) PLA/*m*-SEBS, (c) PLA/EGMA, and (d) TEM image of the PLA/EGMA blend.

Applied Polymer SCIENCE

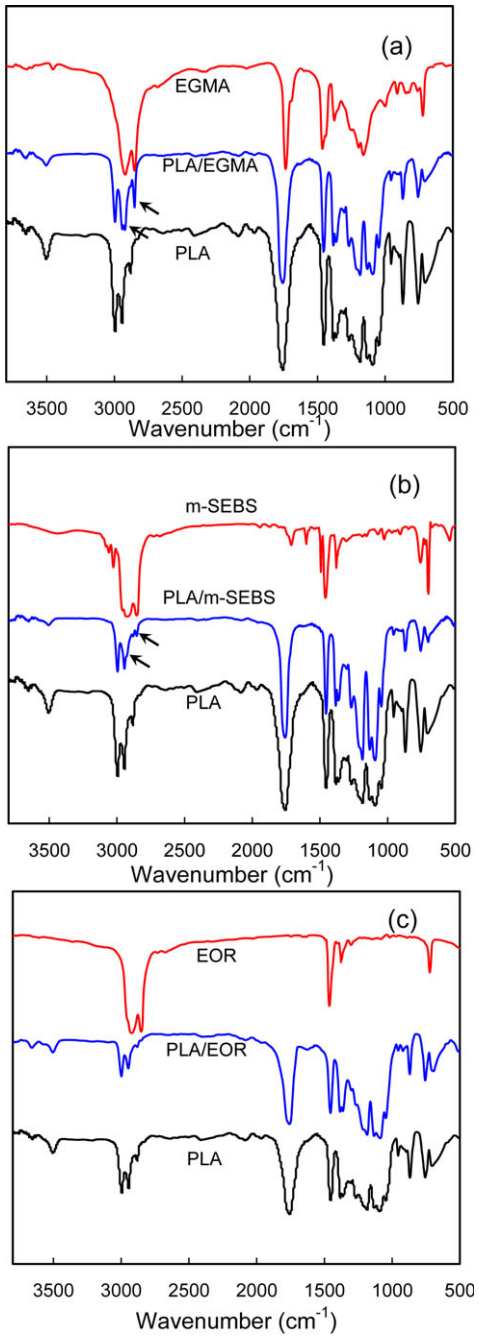

Figure 3. FTIR spectrum of the extracted PLA/rubber blends, (a) PLA/EGMA (removed EGMA by toluene), (b) PLA/*m*-SEBS (removed *m*-SEBS by toluene), and (c) PLA/EOR (removed EOR by heptane). [Color figure can be viewed in the online issue, which is available at wileyonlinelibrary.com.]

For the PLA/EGMA (60/40) blend [Figure 2(c)], the dispersed domain size sharply decreases to 0.5–2 μm. TEM micrographs of the extrusion PLA/EGMA blend are also shown in Figure 2(d), in which OsO_4 preferentially stains the EGMA phase. One can see that the PLA domains are clearly dispersed in the EGMA matrix and there exist many dark spheres with very small size in the PLA domains. Such kind of hierarchical structure is usually observed in reactive blending system. Because the epoxide group on EGMA chains can react with the end carboxyl group of the PLA chain during the melt-mixing, it is believed that a large amount of EGMA-*b*-PLA copolymers are pulled out from their interface to the PLA domains.[7,29] In addition, the morphology that the PLA domains are dispersed in the EGMA matrix is in agreement with a lower viscosity of EGMA at high frequencies as shown in Figure 1.

To further check the possible reaction between PLA and rubber during the melt-blending, FTIR analysis was carried out. Figure 3 displays the FTIR diagrams for the neat PLA, rubber, and PLA/rubber blends. Note that the rubber matrix in all the blend samples has been selectively extracted by hot toluene (for EGMA and *m*-SEBS) or by hot heptane (for EOR) before the FTIR analysis. A type of the —CH_2 symmetrical stretching vibration absorbance at 2850 cm^{-1} and the —CH_2 asymmetrical stretching vibration absorbance at 2930 $cm^{-1}$of EGMA was found in the extracted PLA/EGMA blend, indicating the occurrence of chemical reaction between the end carboxyl groups of the PLA and epoxy groups of the EGMA. A similar phenomenon was also observed in the extracted PLA/*m*-SEBS blend, which suggested the chemical reaction between PLA and *m*-SEBS. In addition, C—H asymmetrical stretching vibration of the benzene ring at 3030 cm^{-1} for *m*-SEBS was not observed in the extracted PLA/*m*-SEBS blend which may be due to the lower resolution of the FTIR. The content of PS block in *m*-SEBS is 28 wt %, and the content of the graft copolymer PLA-*g*-SEBS after blending was also very low. This led to the C—H asymmetrical stretching vibration of the benzene ring can not be observed in the extracted PLA/*m*-SEBS blend. Furthermore, for the extruded PLA/EOR blend, after extracted in hot heptane (remove EOR) for 12 h, a type of the —CH_2 symmetrical stretching vibration absorbance at 2850 cm^{-1} and the —CH_2 asymmetrical stretching vibration absorbance at 2930 cm^{-1} of EOR was not found in the PLA/EOR blend which indicated that the chemical reaction between PLA and EOR was not occurred.

The Morphology of Injection-Molded PLA Blends. Figure 4 shows the SEM images of injection-molded PLA/EOR (60/40) and PLA/*m*-SEBS (60/40) blends near to the skin portion. Because the rubber phase has been selectively etched, one can find that the PLA domains elongate significantly and orientate along the FD. Compared to the EOR system, the orientated microstructure in the injection-molded *m*-SEBS system is much more remarkable and finer. This is well correspondent to the fact that *m*-SEBS is better compatible with PLA.

Figure 5 shows the TEM images of injection-molded PLA/EGMA (60/40) blend both in the FD and in the TD. The dark areas in the pictures represent the rubber domains that are stained by OsO_4 vapor. It is observed that both the PLA and rubber phases are elongated and orientated along the FD and the TD, and they are co-continuous, suggesting the formation of a co-continuous microlayer structure during the injection molding.

In general, the rheology foundation to produce polymer blend with microlayer structure is the flow of binary phase, in which the melt viscosity and elasticity ratio are the most important.[30] We have confirmed that a polymer blend owning the

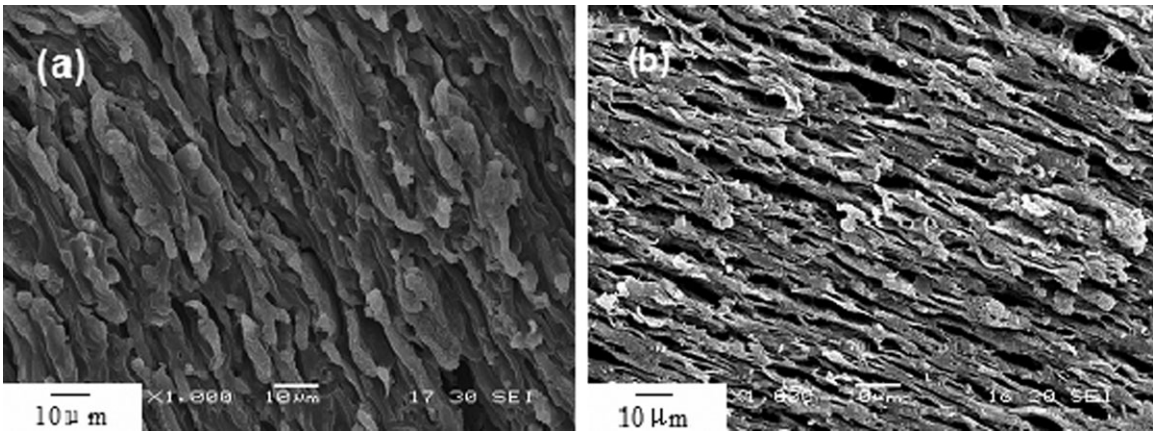

Figure 4. SEM image of the injection-molded (a) PLA/EOR (60/40) (etched by heptane) and (b) PLA/*m*-SEBS (60/40) (etched by toluene) near to the skin portion in FD.

morphology with the plastic as the dispersed phase and the rubber as the matrix is benefit to form the co-continuous microlayer structure during injection molding.[26] A higher viscosity of the plastic phase can delay the break-up time after shear deformation, and thus favors the lamellar orientation. The interfacial compatibility also plays a significant role,[31] because adequate

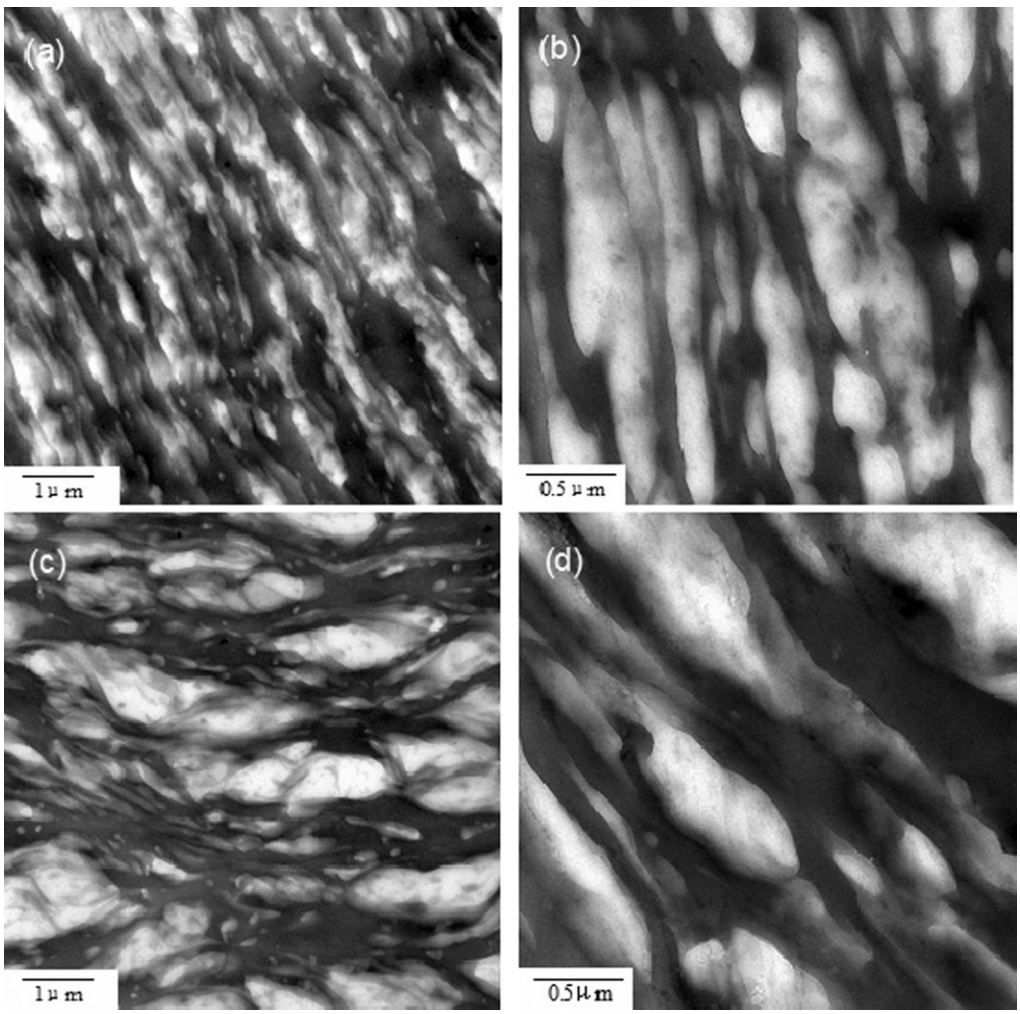

Figure 5. TEM images of the injection-molded PLA/EGMA (60/40) blend stained by OsO_4 vapor near to the skin portion. (a) and (b) in FD, (c) and (d) in the TD. (a) and (c) ×10,000; (b) and (d) ×50,000.

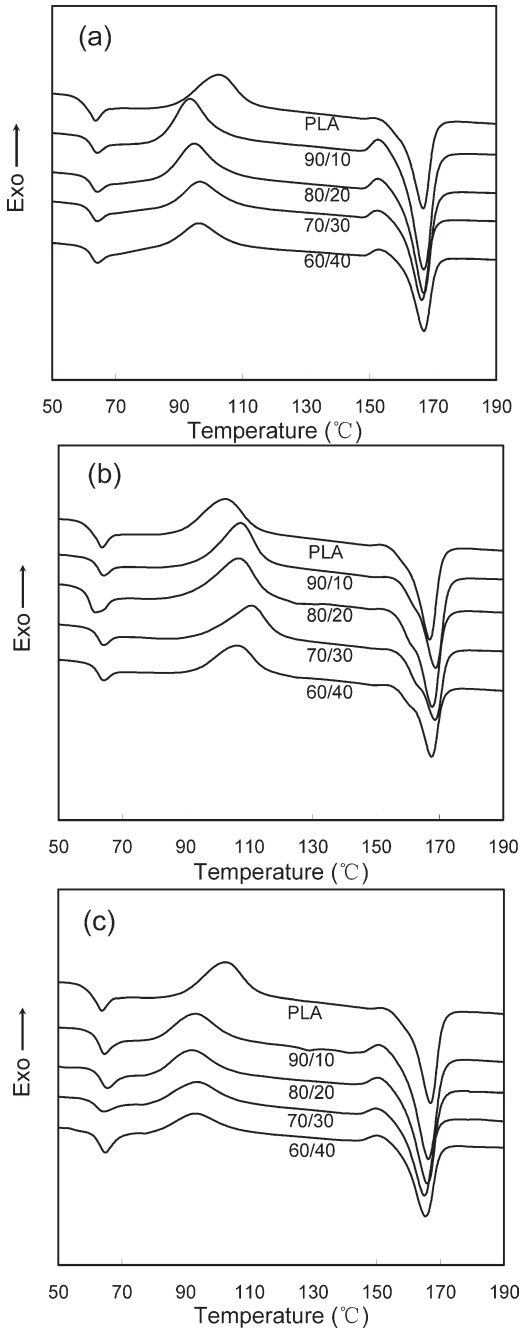

Figure 6. DSC curves of injection-molded PLA and PLA/rubber blends during first heating, (a) PLA/EOR blends, (b) PLA/*m*-SEBS blends, and (c) PLA/EGMA blends.

interfacial force is beneficial for deformation of the dispersed phase. Our experimental results showed that EGMA owns a much low viscosity and a high compatibility to the dispersed PLA domains. This should be the reason of forming the fine co-continuous microlayer structure for PLA/EGMA blend. In the case of PLA/*m*-SEBS (60/40), their viscosities are comparable under the processing condition and the compatibility between them is relatively weak. Although the *m*-SEBS domain can be deformed into the co-continuous layer, the rubber layer is thicker than that in PLA/EGMA. The thickness of the rubber domain in PLA/EOR becomes very large and they are less co-continuous which should be ascribed to the complete incompatibility between PLA and EOR. These differences in morphology should greatly influence the thermal expansion behavior of the PLA/rubber blends.

Crystallization Behavior of PLA Blends

It has been reported that both of the anisotropic thermal expansion and toughness are greatly influenced by the crystallization of polymer blends. Thermal expansion of polymers appears to depend on the orientation degree of the crystallographic axe along the molecular chain direction.[27,28] Ono et al.[27] confirmed the orientation of PP lamellar crystal in the injection-molded PP/rubber blend where a negative CLTE of *c*-axis orients parallel to the FD. Oyama[7] studied the effects of annealing of PLA/EGMA blends on mechanical properties and concluded that the crystallization of the PLA matrix played a significant role on toughening. To clarify whether PLA crystallization has any influence on toughening and reducing thermal expansion in our blend systems, only the DSC data from the first heat scan of the PLA component in the blends were examined, because it is the crystalline state of PLA in the molded samples that could influence the mechanical properties and thermal expansion behaviors of the blends.

Figure 6 shows the DSC first heating thermograms of PLA injection-molded blends with different rubber contents. There is a PLA glass transition at a temperature of about 60°C. All curves show one exothermic peak at 90–110°C due to the cold crystallization of PLA. It should be noted that the cold crystallization temperature (T_c) peaks in PLA/EGMA blends and PLA/EOR blends are located at lower temperatures compared with that in PLA/*m*-SEBS system, probably because there is no obvious heterogeneous nucleation effect of *m*-SEBS on the cold crystallization of PLA matrix. Leu et al.[32] also reported that the addition of *m*-SEBS to PLA matrix can obviously limit the PLA crystallization and lead to weakened cold crystallization ability in PLA.

The calculated crystallinity (X_c) of PLA specimens are shown in Figure 7(a). It can be found that the respective values of X_c for injection-molded PLA/EGMA specimens are 4.8%, 11.8%, 9.7%, 6.6%, and 5.1% for PLA, PLA/EGAM (90/10), PLA/EGAM(80/20), PLA/EGAM(70/30), and PLA/EGAM(60/40). These results indicated the presence of EGMA that facilitates the crystallization of PLA. However, as the content of EGMA in the blend was higher than 10 wt %, the crystallinity of PLA was drastically reduced which could be ascribed to the product of the chemical reaction between the end carboxyl groups of the PLA and the epoxy groups of the EGMA reduced the PLA chain mobility and its ability to crystallize. It can be seen that the crystallinity of PLA in the EOR blends is slightly higher than that in the *m*-SEBS blends. Furthermore, in all the case of PLA/rubber (60/40) blends, the crystallinity of PLA is at the same low level (<10%). Figure 7(b) shows WAXD patterns of injection-molded PLA and PLA/rubber (60/40) blends. A large and broad halo originating from the amorphous region is observed and only a small and broad peak due to the crystalline region is barely visible at ca 16.5° in the blends. In addition, for the injection-molded PLA/rubber blends, typical peaks of the amorphous region of rubbers at higher angles were found compared with the pure PLA. On the basis of the

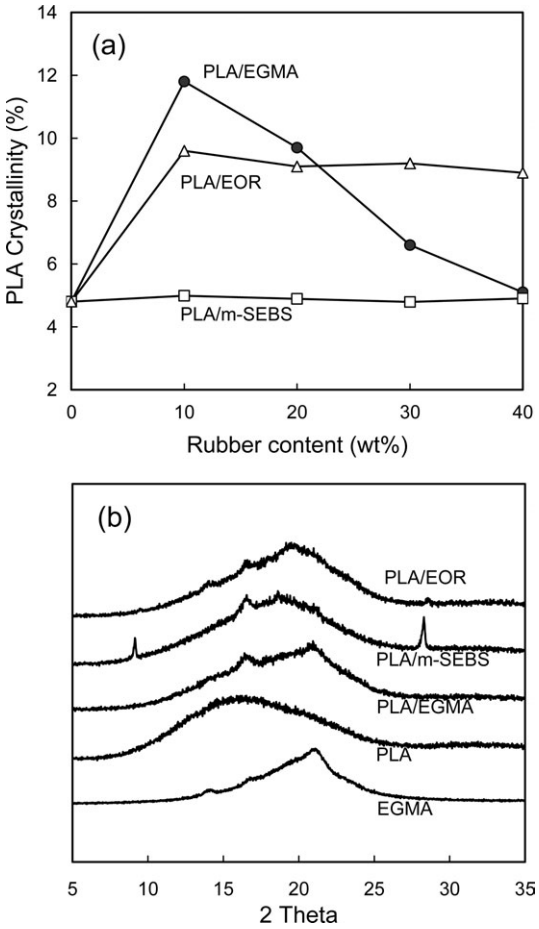

Figure 7. The crystallinity of (a) neat PLA and PLA/rubber injection-molded blends and the WAXD patterns of (b) injection-molded PLA, EGMA, and PLA/rubber (60/40) injection-molded blends.

above results, therefore, the crystallinity of PLA matrix does not appear to be a contributing factor on resulting in the significant dependence of thermal expansion behaviors and impact toughness, especially in the higher rubber loadings region.

Thermal Expansion of PLA/Rubber Blend

Figure 8 shows a typical plot of the normalized linear expansion dL/L in three directions as a function of temperature for the injection-molded PLA blends with 40 wt % EGMA. Because the PLA is little crystallized and its T_g is near to 60°C, therefore the measurement was carried out up to 60°C. The average CLTE over a temperature range from −20 to 60°C in FD, TD, and ND was calculated to be 6.5 × 10^{-5}/°C, 9.8 × 10^{-5}/°C, and 22.5 × 10^{-5}/°C, respectively. It is clear that the specimen formed by injection molding has a low CLTE in FD and TD and a very high CLTE in ND. The average CLTE value in the FD over a temperature range from −20°C to 60°C was calculated and shown in Figure 9. It can be seen that, for the PLA/EOR blends, the CLTE of the injection-molded samples decreases when the EOR concentration is higher than 30 wt %. A similar tendency is observed for PLA/*m*-SEBS blends and PLA/EGMA blends, except for a lower rubber concentration necessary for the drastic reduction of CLTE. One can find that

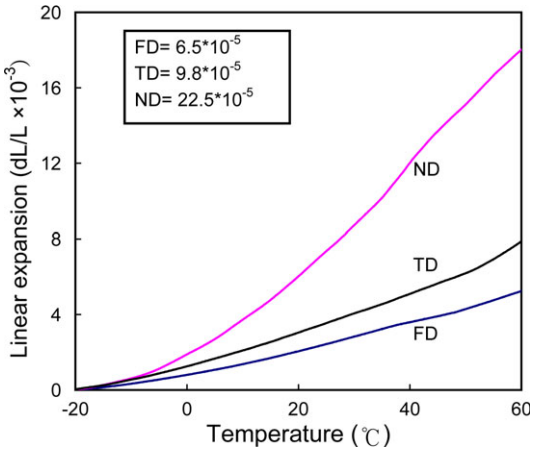

Figure 8. Temperature dependence of the linear expansion for injection-molded PLA/EGMA (40 wt %) in different directions. [Color figure can be viewed in the online issue, which is available at wileyonlinelibrary.com.]

the PLA blended with EGMA gives the lowest CLTE value at a given rubber content.

According to the DSC and WAXD data, the rubber has little effect on the final crystallinity (specifically for PLA/rubber (60/40) blends), and the crystallinity is very small. So the crystal orientation may be not the main driving force to cause the decrease of CLTE. For the PLA/rubber blend, the increase in CLTE at low rubber concentrations should be attributed to the non-continuous rubber domains in the plastic matrices and high thermal expansion of rubber; but when the rubber content exceeds a certain critical value, the CLTE drastically decreases due to the formation of co-continuous microlayer structure. This phenomenon was also observed in PA6/*m*-SEBS and PP/EPR blend.[25] In addition, the different CLTE of PLA/rubber = 60/40 among PLA/EGMA, PLA/*m*-SEBS and PLA/EOR may be attributed to their different microlayer thickness. It can be expected that thinner 3-D continuous microlayers should result in a lower CLTE. Because of this, the viscosity ratio and interfacial compatibility play a significant role in the decrease of CLTE. A decrease in the viscosity ratio and well interfacial compatibility between the

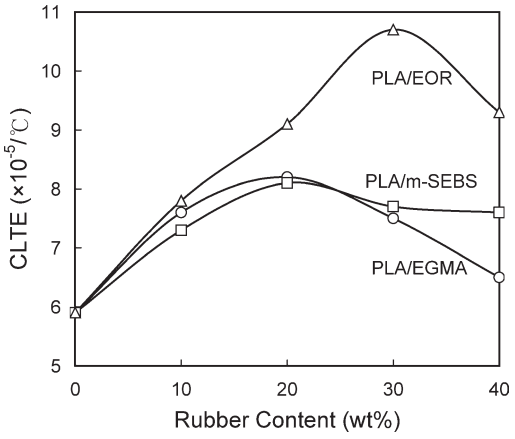

Figure 9. Rubber concentration dependence of the CLTE in the FD for injection-molded PLA/rubber blends.

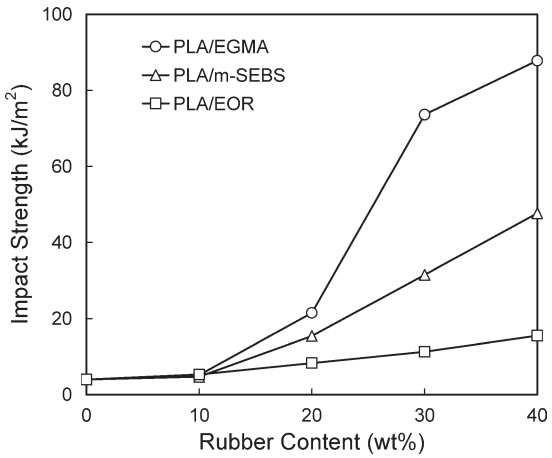

Figure 10. Impact strength of PLA blends as function of rubber content.

rubber and the plastic leads to a lower CLTE of the polymer blend. This is significant because a polymer component with a lower viscosity and suitable interfacial compatibility is easier to deform into microlayers during the injection molding.

Impact Properties of PLA/Rubber Blends

Figure 10 shows the results of notched impact tests. The impact strength of PLA increases with the increase of the rubber content. For PLA/EGMA blends, when the EGMA content is lower than 20 wt %, the improvement in toughness is slight; however, a drastic increase in the impact strength is observed with further increasing the EGMA content. The value for the PLA/EGMA (60/40) blend is 87.8 kJ/m^2, ca. 20 times higher than the neat PLA. This value is much higher than that of PLA/*m*-SEBS and PLA/EOR blends with the same rubber content. Because we have testified to the very low crystallinity of PLA in these polymer blends, the super-toughening effect of PLA/EGMA blends should be ascribed to the better compatilized polymer blends with finer co-continuous microlayer structure.

CONCLUSIONS

We discovered that the CLTE of injection-molded PLA/EGMA blends could be significantly reduced by the addition of 40% rubber component. It was confirmed that 3-D co-continuous microlayer morphologies both for the plastic and rubber are essential for constraining the expansion along FD and TD and a thinner microlayer is helpful to further reduce the CLTE. PLA blends with the notched impact strength over 20 times higher than that of the neat PLA were obtained by reactive blending of PLA and EGMA. The PLA/EGMA blend having high impact resistance and low thermal expansion coefficient simultaneously is of great importance in practical applications.

ACKNOWLEDGMENTS

This research was supported by grants from the National Natural Science Foundation of China (50873033).

REFERENCES

1. Rasal, R. M.; Janorkar, A. V.; Douglas, E. *Prog. Polym. Sci.* **2010**, *35*, 338.
2. Kulinski, Z.; Piorkowska, E. *Polymer* **2005**, *46*, 10290.
3. Wang, Y.; Hillmyer, M. A. *J. Polym. Sci. Part A: Polym. Chem.* **2001**, *39*, 2755.
4. Gajria, A. M.; Dave, V.; Gross, R. A.; McCarthy, S. P. *Polymer* **1996**, *37*, 437.
5. Zhang, G.; Zhang, J.; Wang, S.; Shen, D. *J. Polym. Sci. Part B: Polym. Phys.* **2003**, *41*, 23.
6. Su, Z. Z.; Li, Q. Y.; Liu, Y. J.; Hu, G. H.; Wu, C. F. *Eur. Polym. J.* **2009**, *45*, 2428.
7. Oyama, H. T. *Polymer* **2009**, *50*, 747.
8. Noda, I.; Satkowski, M. M.; Dowrey, A. E.; Marcott, C. *Macromol. Biosci.* **2004**, *4*, 269.
9. Zhang, N.; Wang, Q.; Ren, J.; Wang, L. *J. Mater. Sci.* **2009**, *44*, 250.
10. Jaratrotkamjorn, R.; Khaokong, C.; Tanrattanakul, V. *J. Appl. Polym. Sci.* **2012**, *124*, 5027.
11. Nyambo, C.; Misra, M.; Mohanty, A. K. *J. Mater. Sci.* **2012**, *47*, 5158.
12. Bulota, M.; Hughes, M. *J. Mater. Sci.* **2012**, *47*, 5517.
13. Kwon, O. *J. Soft Matter* **2011**, *7*, 5096.
14. Benoit, C.; Patrick, D.; Francois, F. *Macromol. Biosci.* **2011**, *11*, 1175.
15. Kazuhiro, H.; Shotaro, N.; Takashi, I. *Polymer* **2010**, *51*, 3934.
16. Zhang, J. F.; Sun, X. Z. *Biomacromolecules* **2004**, *5*, 1446.
17. Huneault, M. A.; Li, H. B. *Polymer* **2007**, *48*, 270.
18. Yew, G. H.; Chow, W. S.; Ishak, Z. A. *J. Elastom. Plast.* **2009**, *41*, 369.
19. Trung, N. P.; Niti, S.; Warunee, K. *J. Appl. Polym. Sci.* **2005**, *108*, 393.
20. Yoon, J. S.; Oh, S. H.; Kimb, M. N.; Chin, I. J.; Kim, Y. H. *Polymer* **1999**, *40*, 2303.
21. Tarvainen, T.; Karjalainen, T.; Malin, M.; Pohjolainen, S.; Tuominen, J.; Seppälä, J.; Järvinen, K. *J. Controlled Release* **2002**, *81*, 251.
22. Li, T. N.; Turng, L. S.; Gong, S. Q. *Polym. Eng. Sci.* **2006**, *46*, 1419.
23. Bailey, T. S.; Rzayev, J.; Hillmyer, M. A. *Macromolecules* **2006**, *39*, 8772.
24. Liu, H. Z.; Chen, F.; Liu, B.; Estep, G.; Zhang, J. W. *Macromolecules* **2010**, *43*, 6058.
25. Wu, G. Z.; Nishida, K.; Takagi, K.; Sano, H.; Yui, H. *Polymer* **2004**, *45*, 3085.
26. Wu, G. Z.; Xu, H. B.; Zhou, T. *Polymer* **2010**, *51*, 3560.
27. Ono, M.; Washiyama, J.; Nakajima, K.; Nishi, T. *Polymer* **2005**, *46*, 4899.
28. Kim, D. H.; Fasulo, P. D.; Rodgers, W. R.; Paul, D. R. *Polymer* **2008**, *49*, 2492.
29. Lee, P. C.; Kuo, W. F.; Chang, F. C. *Polymer* **1994**, *35*, 5641.
30. Rodriguez, V. O.; Kamal, M. R. *Adv. Polym. Technol.* **1999**, *18*, 89.
31. Samios, C. K.; Kalfoglou, N. K. *Polymer* **1998**, *39*, 3863.
32. Leu, Y.; Mohd, I. Z.; Chow, W. *J. Appl. Polym. Sci.* **2012**, *124*, 1200.